Design Fundamentals of a ReconfigurableRobotic Gripper System

Ramesh Kolluru, Kimon P. Valavanis, Stanford A. Smith, and Nikos Tsourveloudis

***Abstract*—This paper discusses the design and modeling fundamentals of a multi-degree-of-freedom reconfigurable robotic gripper system (RGS), designed to automate the process of limp material handling, reliably and without distortion, deformation, and/or folding. The reconfigurable gripper design draws upon the authors' previously reported flat surfaced, fixed-dimensions gripper system [1]. The design consists of four arms in a cross-bar configuration, with a flat surfaced, fixed dimensions, suction-based gripper unit mounted on each of the arms. The kinematic and dynamic performance of the reconfigurable RGS is analyzed theoretically and then validated using Integrated Design Engineering Analysis Software (I-DEAS) simulation software.**

***Index Terms*—Apparel, dynamic analysis, limp material, robotic grippers, simulation, static analysis.**

I. Introduction

This paper discusses the design fundamentals of a reconfigurable robotic gripper system (RGS), capable of handling deformable limp material without distortion, deformation and/or folding. The RGS industrial requirements, set by the American Apparel Manufacturer's Association (AAMA) and the Textiles and Clothing Technology Corporation, [TC]^2, are that the system must operate with a reliability of approximately 99%, and, be capable of manipulation rate of approximately 10–12 panels per minute.

As a first step, a prototype flat-surfaced, fixed-dimensions gripper system, shown in Fig. 1, has been built and integrated with commercially available robot manipulators. This prototype design consists of a 9-in $\times$ 12-in rectangular chamber that uses suction to handle material panels whose shape and size match its dimensions. Details of the prototype design, and review of commercial limp material handling devices such as the Walton picker, the Singer gripper and the Clupicker has already been presented in [1] and [2].

The flat-surfaced, fixed-dimensions gripper has been proven capable of exceeding the specified system requirements [1]. However, in order to handle material panels of various shapes, sizes, and weight, a multi-degree-of-freedom RGS has been designed. The RGS consists of four arms in a crossbar configuration, with a miniature version of the fixed dimensions gripper mounted on each of the arms, as shown in Fig. 1. The RGS is required to demonstrate the ability to:

1) manipulate single/multiple panels without distortion, deformation, and/or folding;
2) handle a load of 10 lbs;
3) handle objects of varying shapes and sizes up to 3 ft $\times$ 3 ft;
4) integrate with commercial manipulators (AdeptOne, AdeptThree) robot arms.

The rest of the paper is organized as follows: The overall design is discussed in Section II. A detailed static and dynamic analysis is presented in Section III. Results of theoretical analysis, validated and verified using the Integrated Design Engineering Analysis Software (I-DEAS) simulation software, are presented in Section IV. Theoretical analysis coupled by simulation-based verification justifies the RGS design. Section V concludes the paper.

Manuscript received August 30, 1998; revised November 20, 1999. This work was supported in part by Louisiana Educational Quality Support Fund, Industrial Ties Research Sub-program Grant LEQSF (1996–1999)-RD-B-14, and National Science Foundation, Design, Manufacturing and Industrial Innovation Grant NSF-DMII-9701533. This paper was recommended by Associate Editor R. A. Hess.

The authors are with the Robotics and Automation Laboratory (RAL), The Center for Advanced Computer Studies and Apparel-CIM Center, University of Louisiana, Lafayette, LA 70504 USA.

Publisher Item Identifier S 1083-4427(00)01728-8.

II. Design and Development of the RGS

The RGS mechanism consists of *the gripper system, the robot arm, and the suction generation system*.

A. The Gripper System

The RGS has four arms at right angles to each other in a crossbar configuration. Each arm consists of a linear actuator on which a suction cup is mounted, as shown in Fig. 1. The suction cup may be translated along the length of the arm, under the control of an actuating mechanism, which consists of a stepper motor and a low-level stepper motor controller. The stepper motor controller determines the magnitude and direction of the displacement of the four suction cups. It is possible to control the movement of each of the suction cups independently or in a coordinated manner.

B. The Robot Manipulator

The RGS is integrated with an AdeptThree robot arm, shown in Fig. 1. While designing the RGS, it is necessary to consider the effects of robot accelerations, as justified below.

C. The Suction Generation System

Suction is generated as a consequence of pressure differential developed within the suction cup when a panel of material is held against its surface. The controller determines the amount of suction and activation or deactivation of suction through each of the suction cups. For the system to perform reliably, it is necessary that the suction generated be greater than the weight of the material and overcome the shear forces due to robot accelerations to guarantee grasp stability.

Consider that the robot arm is accelerating at a rate of a_x and a_y in the horizontal and the vertical directions, respectively. The equilibrium of forces in the horizontal and the vertical direction, as shown in Fig. 2, may be resolved as:$\sum F_x = -F_f = ma_x$ and, $\sum F_y = P_g - W - N = ma_y$ where, m is the mass of the material. The frictional force F_f holds the material on the gripper during the translation. The value of the normal force N is determined by the equilibrium of forces in the vertical plane. Consequently, the magnitude of F_f, is determined by the equation,$F_f = \mu N$, where μ is the coefficient of friction.

For grasp stability, it is necessary that $F_x \leq \mu N$. The suction force P_g generated at the suction unit must be sufficient to overcome the slippage effect due to the acceleration of the robot arm, and also the weight and slippage of the material. Further, these equations may be used to determine the minimum effective area of the suction unit, based on the known suction generation capabilities of the generator. It is found that in order to handle the desired payload, the minimum effective area of suction (area of suction cups) should be 5.3 in^2. According to the

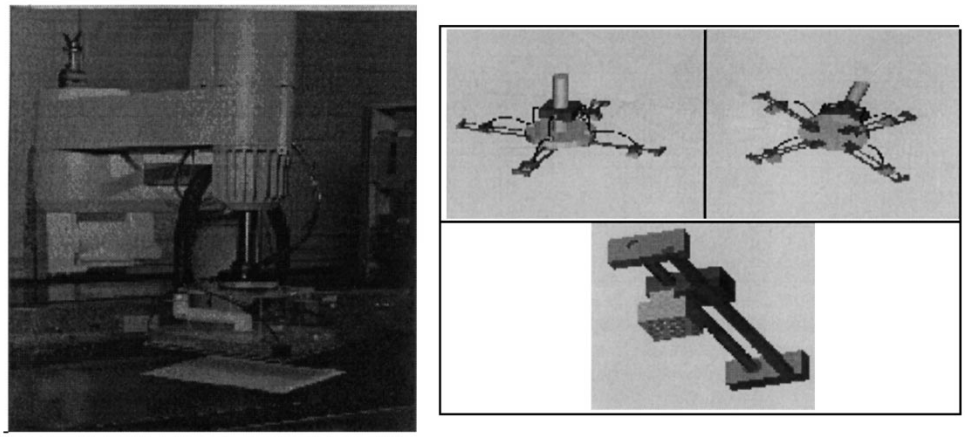

Fig. 1. Prototype fixed-sized (left) and reconfigurable (right) robotic gripper systems.

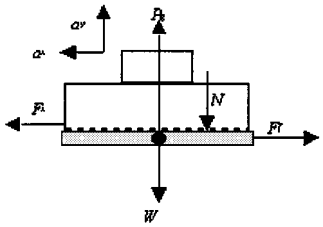

Fig. 2. Forces acting on the material during vertical and horizontal motion.

system requirements, the dimension of the largest object to be handled by the RGS is 3 ft × 3 ft. To accomplish this, the design incorporates a four-arm crossbar configuration, allowing for a 12-in diameter tool flange. A miniaturized version of the existing gripper prototype, weighing less than 2.5 lbs is mounted on each of the arms, serving as the suction cup. A total required payload of 10 lbs is divided amongst the four suction units, contributing to a payload of 2.5 lbs, picked by each suction cup, and an overall load of 5 lbs acting on the lead screw mechanism. The conceptual design parameters of the overall RGS are theoretically validated and then verified, as presented in Section IV. Performance analysis and theoretical validation of the RGS under static and dynamic conditions is presented next.

III. Analysis of the RGS

Kinematic constraints require that the system be considered as a cantilever beam, fully constrained on one end, with a point load—consisting of the gripper self-weight and external load acting on the free end. Static analysis [3] is used to determine the likelihood of system failure due to fatigue stresses, under load. Once the mechanism is proven to be statically robust, dynamic analysis of the mechanism is performed.

A. Static Analysis

Static analysis of the RGS mechanism consists of the following steps:

Step 1) Determine the fatigue strength and yield strength of the mechanism.

Step 2) Calculate the actual torsional and bending stresses developed within the system. If the value of the developed stress is found to be less than the maximum allowable stress, the mechanism is said to be robust.

Step 3) Compute the maximum deflections produced under the given loading conditions and kinematic constraints.

1) Worst Case Stress: "Yielding" failure occurs when the distortion energy at any point on the mechanism exceeds a critical value, as determined by the von Mises stress postulation. The mechanism tends to yield if the combination of stresses exceeds the yield strength of the material. For the selected steel alloy, this value is 36 000 lb/in^2. For mechanisms subject to cyclic loads and accelerations, a factor of safety of 2.0 is generally recommended. Thus, the maximum allowable stress for mechanism is given by: *Maximum allowable stress = Yield stress*/*Factor of safety*. The maximum allowable stress for mechanism is found to be 18 000 lb/in^2, beyond which the mechanism is prone to fail. Since the gripper mechanism will undergo millions of load cycles during its lifetime, the fatigue analysis must be based on infinite life. Fatigue failures occur when the maximum stress developed within the mechanism is greater than the ultimate or tensile strength of the material. The mechanism, subject to cyclic and repetitive loading develops fatigue. The fatigue strength of the mechanism S_e is based on the endurance limit S'_e of the material with which the mechanism is fabricated. The value of S'_e depends on the materials' ultimate tensile strength, S_{UT}, in accordance with the equation: $S'_e = 0.504 * S_{\mathrm{UT}}$. Since the ultimate tensile strength for mild steel is 54 000 lbs/in^2, the endurance limit of the material is 27 216 lbs/in^2. The endurance limit of the mechanism, at room temperature and under no stress concentration conditions, is calculated using $S_e = k_a k_b k_c k_d k_e S'_e$, where k_a, k_b, k_c, k_d, and k_e are mechanism specific constants such as surface finish factor, size factor, load factor, temperature factor, and fatigue stress concentration factor, respectively. The value of the mechanisms' endurance limit has been found to be 14 204 lbs/in^2, at which fatigue failures are possible. Since the loading involves stress fluctuations about a non-zero mean value, additional analysis is performed to determine actual stresses developed.

2) Actual Stresses Developed in the RGS: The effect of an external load on the gripper is similar to the effect of an external point load on a cantilever, fixed at one end, and free at the other. The effects of bending stresses due to external and internal loads and torsional stresses due to the motor are evaluated. Consider the situation in which an external load acts on the cantilever beam aside from the uniformly distributed self-weight of the beam. This results in a bending stress,σ, calculated as $\sigma = (FL + x\pi/4d^2\rho L(L/2))/(\pi/32d^3)$, where the length of the lead screw is 12 in, diameter is 0.5 in, and specific weight of mild steel is 0.283 lb/in^3. Based on loading characteristics, the maximum bending stress, σ_1 is found to be 5248 lbs/in^2, while the minimum bending stress, σ_2 is found to be 2786 lbs/in^2, well within tolerance limits. The

torsional stress induced in the mechanism because of motor torque may be calculated as $\tau_{xy} = 16T/\pi d^3$, where d is the diameter of the beam, and T is the torque generated by the motor. The value of torque (from motor specifications) is 2.187 lb-in. By substituting into the equation, the torsional stress has been calculated as 89.63 lb/in^2. The combined stress, σ' due to bending and torsional stresses (von Mises minimum distortion-energy theory) may be determined using the equation: $\sigma' = \sqrt{\sigma^2 + 3\tau_{xy}^2}$. The value of $\sigma'_{\max}$ was found to be 5250 lb/in^2, and the value of minimum overall stress,$\sigma'_{\min}$ was found to be 2790 lb/in^2. As stated earlier, the yield strength for the selected material is 36 000 lbs/in^2. Thus the maximum stress of 5250 lb/in^2 gives a factor of safety of 6.86 Since this is greater than the minimum required safety factor of 2.0, ***the system may be considered safe with regard to yielding***. The mechanism's mean, σ_{mean} and alternating, σ_{alt} stresses may be determined as: $\sigma_{\text{mean}} = (\sigma'_{\max} + \sigma'_{\min})/2$, and, $\sigma_{\text{alt}} = (\sigma'_{\max} - \sigma'_{\min})/2)$. The mean stress alternating stress values were found to be 4020 lbs/in^2 and 1230 lbs/in^2. The alternating stress value needs to be less than the maximum allowable alternating stress, S_a, at which the mechanism is prone to fail due to cyclic loading. This value is calculated using the following equation: $S_a = (S_{\text{UT}} * S_e)/(S_{\text{UT}} + S_e * (\sigma_{\text{mean}}/\sigma_{\text{alt}}))$. From this equation, the value of maximum allowable alternating stress, S_a, was found to be 7568 lbs/in^2. Since the developed alternating stress σ_{alt} due to cyclic loading was found to be only 1230 lbs/in^2, ***the designed mechanism may be considered safe from fatigue stresses***, with a factor of safety of 6.15.

3) Maximum Deflections due to Static Loading: The self-weight of the steel cantilever beam may be computed as: *Weight of beam* $= (\pi d^2 \rho L)/4$. It has been found that the total weight of the beam is 0.66 lbs, which may be considered as a uniformly distributed load (UDL) of 0.055 lbs/unit length of the beam. Further, a point load of a maximum of 5 lbs may be acting upon the cantilever. These loads will cause deflections of the beam which need to be low in order to obtain good positioning accuracy and reliability. Deflections resulting due to the self-weight of the beam are computed as follows: $\delta_{\text{self}} = wL^4/8EI$, where w is the UDL due to the beam self-weight, L is the length of the beam, E is the Young's modulus of elasticity for steel, and I is the moment of inertia of the cylindrical beam. The value of deflection has been found 0.0015 in. Deflection of beam due to an external point load on the cantilever is given by: $\delta_{\text{point}} = WL^3/3EI$, where W is the external point load of 5 lbs, acting on the beam. The deflection due to external load has been calculated as 0.031 in. The overall deflection is given by the sum: $\delta_{\text{total}} = \delta_{\text{point}} + \delta_{\text{self}}$. It was numerically found that the total deflection of the beam is 0.0325 in, which is adequate for the pick and place operation for which the system is being designed.

B. Dynamic Analysis

Dynamic analysis [4] has been performed in order to determine the behavior of the system, under the effect of external loads and forces. The steps involved consist of:

- Step 1) Determine the natural frequency of the mechanism: compute normal modes of vibration, and, damped/resonant frequency of the mechanism.
- Step 2) Evaluate the effect of acceleration of the robot on the performance of the system: compute dynamic displacements and resultant dynamic stresses resulting from robot arm acceleration.
- Step 3) Compute the logarithmic decrement to determine the rate of decay of oscillations due to external disturbances.

1) Natural Frequency: All systems possessing mass and elasticity are capable of free vibration when disturbed. The frequency with which the body vibrates is known as the natural frequency of the system. The natural frequency is a function of the mass and stiffness of the system. The natural frequency for undamped, free vibrations of the mechanism is given by: $\omega_n = \sqrt{k/M_{\text{eff}}}$, where k is the stiffness and M_{eff} is the effective mass of the system. The stiffness, k, for a cantilever beam fixed at one end is given by the following equation: $k = 3EI/L^3$ where E is the Young's modulus of elasticity for steel, I is the moment of inertia and L is the length of the beam. The value of k is found equal to 154.46 lbs/in. The next step is to determine the effective mass of the system under two conditions:

1) when the gripper is unit is unloaded, thus only a 2.5-lb self-weight of the gripper is acting on the cantilever;
2) the cantilever has an additional 2.5 lbs payload due to the object picked by the gripper.

For the unloaded case, $M_{\text{eff}} = 0.00758$ lb-s^2/in. Substituting $W = 5$ lbs for the loaded case, we find that $M_{\text{eff}} = 0.0141$ lb-s^2/in. Once, the effective mass is computed, the natural frequency may be calculated. In accordance with the above, the natural frequency of the mechanism under no external load conditions is found to be 142.60 rad/s or 22 cycles/s. With an additional 2.5-lb load mounted on the mechanism, the natural frequency is found to be 104.77 rad/s, or 16 cycles/s. For damped vibrations, we have $\omega_d = \omega_n\sqrt{1-\zeta^2}$ where ω_d is the damped frequency or the resonant frequency of the mechanism with a damping factor ζ. Assuming a conservative value of 0.1 for damping, we find the unloaded and the loaded damped frequencies of the system to be 141.88 rad/s and 104.24 rad/s. If the mechanism starts to vibrate at these frequencies under the effect of external forces, resonance could occur.

Next, we determine the dynamic displacements, due to the acceleration of the robot arm. Let a_V and a_H represent the maximum acceleration of the robot in the vertical and horizontal plane. It is experimentally found that the a_V is 77.16 in/s^2 and a_H is 379.85 in/s^2. The effective forces F_V and F_H are found to be 1.09 lbs and 5.35 lbs, respectively. Dynamic displacements represent the maximum amplitude of oscillation of the mechanism from its mean position. The peak response to an excitation of magnitude F_0 is

$$x = \frac{F_0}{k}\left[1 - \frac{e^{-\zeta\omega_n t}}{\sqrt{1-\zeta^2}}\cos(\sqrt{1-\zeta^2}\omega_n t - \varphi)\right]$$

where F_0 is the exciting force (F_V or F_H), ω_n is the natural frequency, and φ is the phase angle, given by: $\tan\varphi = \zeta/\sqrt{1-\zeta^2}$. The maximum dynamic displacement in vertical and horizontal planes is found to be 0.0252 in and 0.0051 in, respectively. Dynamic displacements vary over a period of time, as a function of the damping present in the system. The larger the value of damping, the faster the rate decay of free oscillations. The value of logarithmic decrement, represented by δ, is used to quantify the rate of decay. The logarithmic decrement, represented as the natural logarithm of the ratio of any two successive amplitudes, depends on the damping coefficient. Thus, $\delta = \ln(x_1/x_2) = \pi\zeta/\sqrt{1-\zeta^2}$. Substituting $\zeta = 0.1$, we find that $\delta = 0.6315$; the amplitude ratio of two consecutive cycles is $x_1/x_2 = e^{\delta} = e^{0.6315} = 1.8804$. This indicates that between two successive cycles, the value of dynamic displacement decreases by a factor of 0.531802. Since the mechanism frequency is 16 to 22 cycles/s, it is evident that the initial maximum dynamic displacement of 0.0252 in reduces to less than half within $1/16$th of a second. It is evident that within much less than 1 s, the dynamic displacements in the horizontal and vertical directions will subside, and become negligible. Thus, there is no need for any additional delays or dwell period between two successive pick and place cycles of the RGS.

To summarize, the design is found to be capable of mechanically sound and robust behavior under static and dynamic conditions. Although the design is proven to be mathematically robust, further validation and verification is performed using a finite element tool called

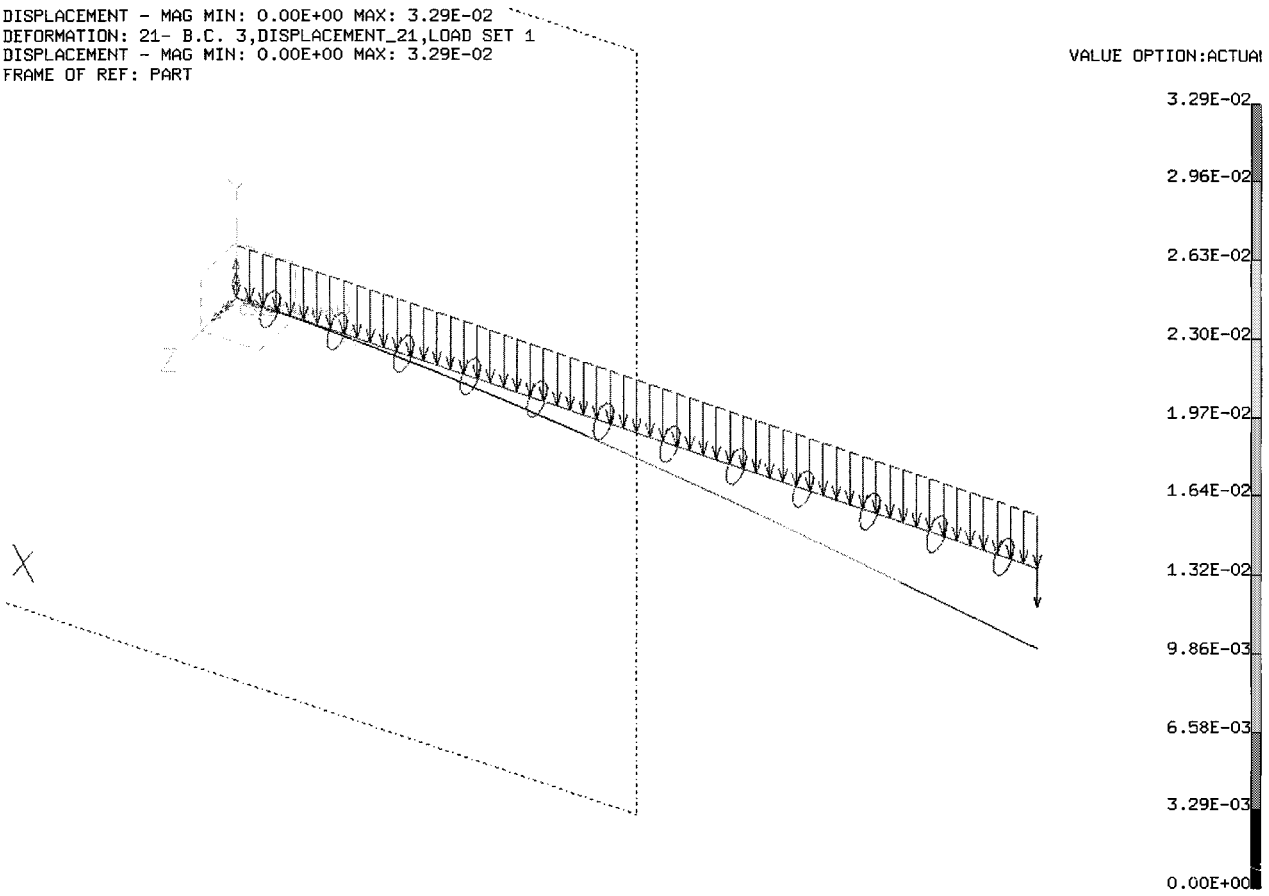

Fig. 3. Deflection of the beam due to load and self-weight (maximum deformation: simulation—0.0329 in).

Integrated Design Engineering Analysis Software (I-DEAS) software package [11], widely used for modeling, design, and analysis of mechanisms.

IV. Simulation Analysis and Results

Finite element analysis of mechanisms consists of the following three steps:

Step 1) pre-processing
Step 2) solution
Step 3) post processing.

1) Pre-Processing: This consists of three processes discussed in the following.

a) Creating the model: The purpose of finite element modeling is to build a model that behaves mathematically like the structure being modeled. A finite element model has been created using beam elements.

b) Meshing: The model has been meshed using beam elements. There are 12 beam elements along the length of the model of the mechanism.

c) Boundary conditions: A UDL has been applied on all the elements along the length of the beam, which represents the self-weight of the mechanism. After specifying the constraints and loads, a "load set" is created, which has a list of all the constraints, restraints and loads on the model. This load set is used for the calculations while solving the model.

2) Solution: The finite element model is solved. Finite element modeling divides the structure into a grid of elements, which model the real structure. Displacements of the nodes and the stresses in each element of the node are calculated. During dynamic analysis, the natural frequencies and normal modes of vibration are determined.

3) Post-Processing: In the post processing step, all results are displayed.

The analysis has first been carried out considering the drive mechanism as a cantilever beam of length 12 in and having a diameter of 0.5 in. The following are the steps involved in the analysis:

1) A UDL equal to the weight of the beam has been applied on the model. According to the finite element solution, the deflection has been found to be 0.00155 in. From theoretical calculations, the deflection due to self-weight of the lead screw has been obtained as 0.0015 in, which validates the result. Next, a point load of 5 lbs has been applied on the free end of the lead screw, in addition to the self-weight of the mechanism. The deflection in this case has been found to be 0.0329 in, as shown in Fig. 3, corroborating theoretical value of 0.031 in.
2) The stress obtained from the analysis, shown in Fig. 4, is found to be 5210 lbs/in^2, while stresses from theoretical results have been found to be 5250 lbs/in^2.
3) For the dynamic analysis, the loads applied on the body are not considered for determining the natural frequencies and the normal modes of vibration. Solving the model yields the following modes of vibrations and corresponding natural frequencies. The 1st mode of vibration is shown in Fig. 5.

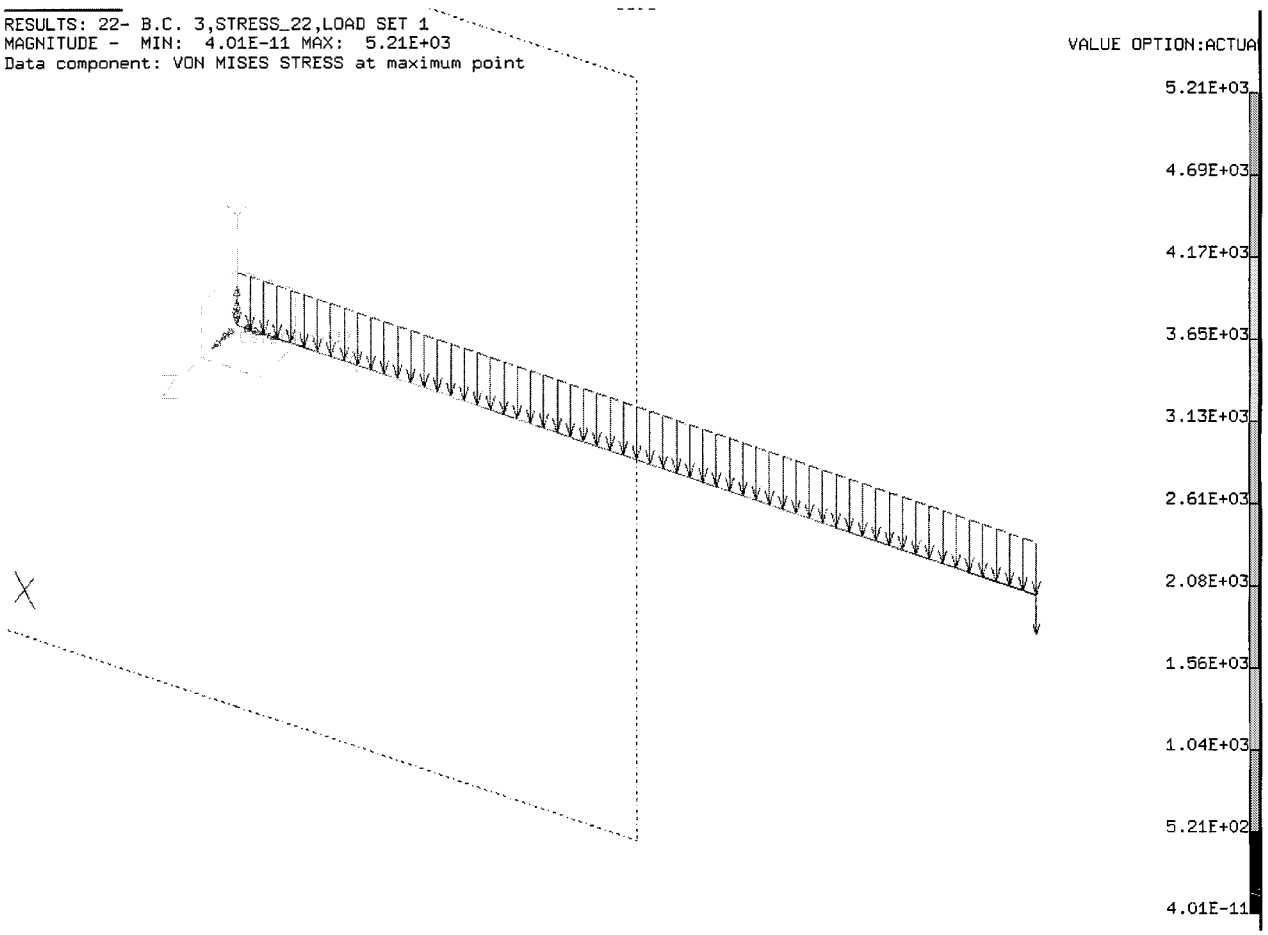

Fig. 4. Stress acting on beam due to load and self-weight (maximum stress: simulation—5210 lbs/ in^2).

TABLE I
THE FIRST SIX NORMAL MODES

Normal Mode of Vibration	Natural Frequency
First/Second	98.24
Third/Fourth	254.14
Fifth/Sixth	612.16

From Table I, we conclude that the predominant mode is the first mode (frequency of 98.24 rad/s). The damped frequency is 98.73 rad/s, which should to be avoided during excitation, to prevent resonance. These values correspond to theoretically derived values of 104.77 rad/s (natural frequency), and 104.24 rad/s (resonant frequency).

To avoid resonant vibrations due to periodic motion of the robot arm, vibrations from the first cycle should diminish before the vibrations due to the second cycle get super-imposed on the previous one. The time lag required between two cycles is determined by the logarithmic decrement, which is defined as the natural logarithm of any two successive amplitudes. Considering the ratio between two successive amplitudes to be 5%, the time lag between two successive cycles may be calculated as: $x_1 = x_2 e^{-\zeta \omega_n t}$ where x_1 and x_2 are the values of two successive amplitudes, ζ is the damping ratio, ω_n is the natural frequency, and t is the time period of the vibration. From the above equation, the time required for vibrations due to robot arm accelerations to die down has been calculated to be less than $1/16$th of a second. It is evident from the foregoing, that the effect of accelerations of the robot arm on the vibrations of the RGS is minimal, and that the RGS is dynamically stable.

V. DESIGN SPECIFICATIONS

In summary, the theoretical analysis coupled by simulation-based verification justifies the RGS design with accurately derived design parameters, as summarized in Table II.

VI. CONCLUSION

The design and modeling fundamentals of a reconfigurable robotic gripper have been presented. The design of the system has been analytically validated for static and dynamic behavior that the RGS may be subjected to in normal operational conditions. The design of the system has been proven mechanically robust and stable. Further validation of the system design has been provided by the use of I-DEAS simulation software. A fully validated design for the RGS mechanism has been derived. The overall reconfigurable gripper system design has been proven kinematically and dynamically robust, indicating that the gripper, once developed, will be capable of reliable manipulation of limp material. The analytical study has resulted in defining parameters for the fabrication of a reconfigurable gripper, currently under development.

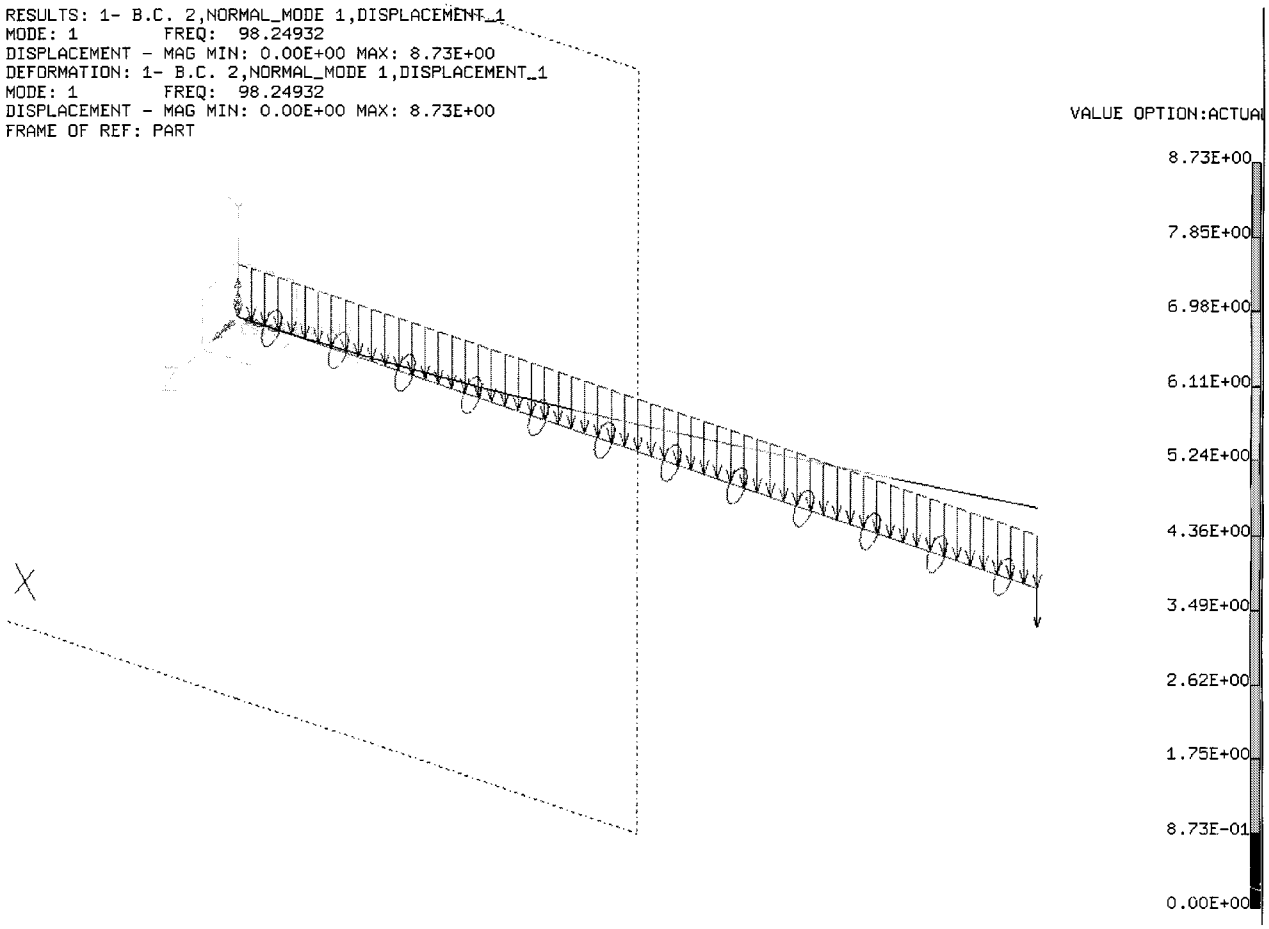

Fig. 5. First normal mode of vibration (natural frequency: simulation—98.249382 rad/s).

TABLE II
DESIGN PARAMETERS OF THE RGS MECHANISM

Length of each arm (L)	12 inches	
Diameter of each arm (d)	0.5 inches	
Payload on each arm	Max. 5 lbs	
Maximum stress (Loaded)	Theoretical: 5250 lb/in^2;	Simulation: 5210 lb/in^2
Maximum deflections (Unloaded)	Theoretical: 0.0015";"	Simulation: 0.00155
Maximum deflections (Loaded)	Theoretical: 0.031";	Simulation: 0.0329"
Natural frequency of each arm	Theoretical: 98.24 rad/sec;	Simulation: 104.77 rad/sec
Damped frequency of each arm	Theoretical: 98.73 rad/sec;	Simulation: 104.24 rad/sec

REFERENCES

[1] R. Kolluru, K. P. Valavanis, and T. Hebert, "Modeling, analysis and performance evaluation of a robotic gripper for limp material handling," *IEEE Trans. Syst., Man, Cybern.*, vol. 20, pp. 480–48, 1998.

[2] T. Hebert, K. P. Valavanis, and R. Kolluru, "A real-time hierarchical sensor-based robotic system architecture," *J. Intell. Robotic Syst.*, vol. 7, pp. 1–27, 1997.

[3] J. E. Shigley, *Engineering Design*, 3rd ed. New York: MacGraw-Hill Series in Mechanical Engineering, 1977.

[4] W. T. Thomson, *Theory of Vibration with Applications*, 3rd ed. Englewood Cliffs, NJ: Prentice-Hall, 1988.

[5] D. Dubois and H. Prade, *Fuzzy Sets and Systems: Theory and Applications*. New York: Academic, 1980.

[6] D. Driankov, H. Hellendoorn, and M. Reinfrank, *Introduction to Fuzzy Control*. New York: Springer-Verlag, 1996.

[7] *Fuzzy Logic Toolbox User's Guide*. Natick, MA: The Math Works, Inc., 1998.

[8] W. S. Janna, *Introduction to Fluid Mechanics*. Boston, MA: PWS Eng., 1987.

[9] P. N. Modi and S. M. Seth, *Hydraulic and Fluid Mechanics*, 10th ed. New Delhi, India: Standard Book House, 1991.

[10] N. C. Tsourveloudis, R. Kolluru, and K. P. Valavanis, "Fuzzy control of suction-based robotic gripper systems," presented at the 1998 IEEE Int. Conf. Control Applicat., Trieste, Italy.

[11] M. H. Lawry, I-DEAS Master Series Mechanical CAE/CAD/CAM Software, Structural Dynamics Research Corporation (SDRC), OH, 1993.

[12] N. C. Tsourveloudis, R. Kolluru, K. P. Valavanis, and D. Gracanin, "Suction Control of a Robotic Gripper: A Neuro-Fuzzy Approach," *J. Intell. Robotic Syst.*, vol. 9, pp. 1–21, 1999.

Mobile Robot Navigation in 2-D Dynamic Environments Using an Electrostatic Potential Field

Kimon P. Valavanis, Timothy Hebert, Ramesh Kolluru, and Nikos Tsourveloudis

***Abstract*—This paper proposes a solution to the two-dimensional (2-D) collision free path planning problem for an autonomous mobile robot utilizing an electrostatic potential field (EPF) developed through a resistor network, derived to represent the environment. No assumptions are made on the amount of information contained in the a priori environment map (it may be completely empty) and on the shape of the obstacles. The well-formulated and well-known laws of electrostatic fields are used to prove that the proposed approach generates an approximately optimal path (based on cell resolution) in a real-time frame. It is also proven through the classical laws of electrostatics that the derived potential function is a global navigation function (as defined by Rimon and Koditschek [11]), that the field is free of all local minima and that all paths necessarily lead to the goal position. The complexity of the EPF generated path is shown to be $O(mn_M)$, where m is the total number of polygons in the environment and n_M is the maximum number of sides of a polygonal object. The method is tested both by simulation and experimentally on a Nomad200 mobile robot platform equipped with a ring of sixteen sonar sensors.**

***Index Terms*—Electrostatic potential field, mobile robots, navigation.**

Manuscript received August 15, 1998; revised November 20, 1999. This work supported in part by NSF Grants BES-9506771 and BES-9712565. This paper was recommended by Associate Editor R. A. Hess.

K. P. Valavanis, T. Hebert, and R. Kolluru are with the Robotics and Automation Laboratory, The Center for Advanced Computer Studies, University of Louisiana Lafayette, Lafayette, LA 70504 USA.

N. Tsourveloudis was with the Robotics and Automation Laboratory, The Center for Advanced Computer Studies, University of Louisiana Lafayette, Lafayette, LA 70504 USA. He is now with the Department of Production Engineering and Management, Technical University of Crete, 73100 Chania, Greece.

Publisher Item Identifier S 1083-4427(00)01727-6.

I. INTRODUCTION

This paper proposes an Electrostatic Potential Field (EPF) based solution to the Mobile Robot (MR) path planning and collision avoidance problem in two-dimensional (2-D) dynamic environments. The EPF is obtained in four steps:

1) create an *occupancy map* of the environment;
2) create the corresponding *resistor network* that is representative of the MR's operational environment;
3) create the *conductance map* from the resistor network;
4) solve the resistor network to obtain the *potential field*.

The laws of electrostatic fields are used to prove that the proposed approach generates in real-time a local minima free *minimum occupancy* approximately optimal path, and that all generated paths necessarily lead to the goal position. No assumptions are made on the amount of information contained in the environment *a priori* map; the map may be (initially) completely empty. However, a complete sensor based model of the environment is built and information from environment maps is combined with on-line sonar sensor data, to plan, replan and execute a collision free path in real-time. The resolution of the environment map depends on the "size" of the smallest possible square cell in the grid. The MR is modeled as a "point" about its center of mass; hence, the 2-D workspace and the configuration space coincide. The MR is treated as a "point source" where current is injected into it to compute the adjacent cell resistances. Further, no assumptions are made on the shape of obstacles, their location and their velocities. Obstacles are stored as a collection of line segments with their half-planes intersecting to form the obstacle area. Obstacles are modeled as areas of high resistance within an area of low resistance; thus, areas of high obstacle occupancy are mapped to high resistances and areas containing relatively few obstacles are mapped to low resistances. Completely occupied cells of the network are modeled as an infinite resistance (open circuit). The cell the robot is assigned to is treated as an "empty cell" with no object, so the robot may move through and out of the cell. With a maximum potential at the robot's initial position and the sole minimum at the desired goal point, an EPF is created in which most of the current flow is in areas of (least) minimum resistance, corresponding to a path of minimum occupancy in the real environment while moving to the goal point. Stated differently, the optimum path minimizes the sum of swept occupancies (the total swept occupancy); the MR is pushed away from the boundary of obstacles while being attracted towards the goal position. It is shown that the complexity of the EPF generated path is linear with respect to the number of obstacle edges within the environment, $O(mn_M)$, where m is the total number of polygons in the environment and n_M is the maximum number of sides of a polygonal object.

The rest of the paper is organized as follows: Section II summarizes related work and discusses the fundamental laws of electrostatic potential fields, used as justification for the proposed solution. Section III presents the path planner solution, Section IV identifies similarities of the proposed approach with dynamic programming, and Section V presents simulation and real-time results. Section VI concludes the paper.

II. RELATED WORK AND BACKGROUND INFORMATION

A. Related Work

Most solution approaches to the MR navigation problem recommend global navigation (generating a path leading to the goal point) and local navigation (follow the global path avoiding collisions with obstacles). A survey of techniques used for navigational planning along with a